

High Retention Rate NCA Cathode Powders from Spray Drying and Flame Assisted Spray Pyrolysis Using Glycerol as the Solvent

Jianan Zhang, Siqi Xu, Khaleel I. Hamad, Ahmed M. Jasim, and Yangchuan Xing*

Department of Biomedical, Biological, and Chemical Engineering, University of Missouri, Columbia, Missouri 65211, USA

*Corresponding author email: xingy@missouri.edu

Abstract

This paper reports the synthesis of $\text{LiNi}_{0.8}\text{Co}_{0.15}\text{Al}_{0.05}\text{O}_2$ (NCA) cathode powders using a simple flame assisted spray pyrolysis (FSP) and a spray drying (SD) processes, in which metal salt precursors dissolved in glycerol were used for spraying. X-ray diffraction confirms that the NCA powders have a layered structure, with a low order of cationic mixing. Electron microscopy shows that the particles produced by FSP have a relatively smaller size and a smoother surface than that produced by SD. The NCA powder from the FSP process has an initial discharge capacity of 200.2 mAh/g in voltage range of 3.0 – 4.3V at 0.1C. It shows very good capacity retention of 91.5% at 1C and 89.4% at 5C after 200 cycles. These results demonstrate that glycerol can replace water and be used as a solvent in spray processes to make cathode powders, promising a new environmentally-friendly synthesis route for battery powder materials production.

Keywords: Cathode material, NCA powders, Glycerol, Flame-assisted spray pyrolysis, Spray drying

1. Introduction

Nickel-rich cathode materials are promising candidates for Li-ion batteries and have been made in different production processes [1, 2]. Different methods have been reported, including solid state [3, 4], co-precipitation [5], sol-gel [6], solution combustion [7], spray drying [8-10], and spray pyrolysis [10-14]. Compared with other techniques, the spraying processes usually have a relatively simple procedure and are considered as a promising route for continuous large-scale production of powder materials at a low cost. Previous spraying methods for producing NCA powders include three routes. The first is a solid-state reaction route assisted by spray drying, which was also mentioned as a ball milling-spray drying process [8, 9]. The second is a two-step solution spray pyrolysis method, in which spray pyrolysis was used to produce Ni-Co-Al-O precursor first, and then lithiation was conducted in a second step [11, 14, 15]. The third is a solution spray drying method, in which all metal salts were dissolved in an aqueous solution to produce the powder with desired components [10]. In general, spraying methods using a solution is much simpler than the solid-state reaction route. For example, to get a desired electrochemical performance, the solid-state method needs an extra step of pressure treatment before heat treatment [8] or a long annealing process (e.g., 28 hours) [9]. In contrast, when using a solution process, there is no special need for heat treatment and the annealing time is much shorter (~ 12 hours). Furthermore, the solution spray method can often achieve desirable mixing and uniformity of all components during the powder synthesis process.

Although solution spray processes have been used to successfully synthesize NCA, extra efforts are needed to achieve desired electrochemical performance. In previous work, there needs an extra step of solid-state reaction for lithiation [11, 14, 15]. When using deionized water as the solvent, organic additives [11] or chelating agents [10] were needed. To develop a new spray

process with new solution preparation for synthesizing NCA, we have used glycerol as the solvent to replace deionized water. It has been demonstrated in previous work in a non-spraying thermal decomposition process that glycerol as a solvent is able to produce cathode materials with desired electrochemical performance [16, 17]. Since glycerol is a main byproduct in the bio-diesel production processes, it can be obtained from renewable and sustainable sources and is environmentally friendly [18]. Glycerol is itself a fuel, and its combustion can provide heat energy for materials processing. This was demonstrated in the flame-assisted spray pyrolysis (FSP) to make NCA powders. As a comparison, NCA cathode powders were also made with only spray drying (SD) without a flame. It was demonstrated that the powders from the FSP process had a much better performance than that from the SD process.

2. Experimental

2.1. Material synthesis

Fig. 1 shows a schematic of our FSP process, in which the flame zone involves the combustion of natural gas, as well as the glycerol evaporated from the precursor. For the SD process, this flame zone was turned off and there is only the drying zone. Powder collection was achieved through a cyclone and cartridge filters. The nozzle is a two-fluid nozzle with oxygen as the atomizing gas.

The precursor was prepared by first mixing metal salts, $\text{LiCH}_3\text{COO}\cdot 2\text{H}_2\text{O}$, $\text{Ni}(\text{CH}_3\text{COO})_2\cdot 4\text{H}_2\text{O}$, $(\text{CH}_3\text{COO})_2\text{Co}\cdot 4\text{H}_2\text{O}$, and $\text{Al}(\text{NO}_3)_3\cdot 9\text{H}_2\text{O}$, with vegetable glycerol in a glass beaker. The mixture was then stirred at 80 °C for 4 ~ 6 hours to form a clear solution. The Li:Ni:Co:Al molar ratio was set to 1.15:0.8:0.15:0.05 and the total metal concentration of the glycerol precursor solution was 3M. The extra lithium salt was used to compensate for the loss during the synthesis process. The prepared precursor solution was then fed to the nozzle with

heating to reduce the viscosity of the precursor fluid. As shown in Fig. 1, spray droplets produced from the nozzle first went through the drying zone. The temperature of the drying zone was controlled to 270 °C. The droplets became semi-dry powders after the drying zone, which then entered the flame zone where they were further processed. When only the SD process was used, the pilot flames were turned off so only the dried powder was collected without further processing. The samples collected from both FSP and SD processes were further annealed at 750 °C for 7 hours in a tube furnace under oxygen atmosphere.

2.2. Powder characterization

A scanning electron microscope (FEI Quanta 600 FEG) was used to examine the morphology of the prepared samples. The crystalline structure of the synthesized samples was examined by an X-ray diffractometer (XRD, PANalyticalX'Pert) with monochromatic and nickel filtered $\text{CuK}\alpha$ radiation ($K_{\alpha 1} = 1.540598 \text{ \AA}$ and $K_{\alpha 2} = 1.5444 \text{ \AA}$). The XRD data were collected in the 2θ range from 10° to 80° with a scanning step of $0.02^\circ \text{ s}^{-1}$. The specific surface area of different powders was calculated by Brunauer-Emmett-Teller (BET) analysis method using a surface area analyzer (Beckman Coulter SA 3100).

2.3. Electrochemical characterization

The powders were tested in coin cells (CR2032) as cathode materials. The electrodes were first prepared by making a slurry that contains 80 wt% active material of the synthesized powder, 10 wt% carbon black (Vulcan XC72, Cabot), and 10 wt% polyvinylidene fluoride (average MW $\sim 534,000$, Sigma-Aldrich) binder in N-methyl-2-pyrrolidinone. The slurry was cast on an aluminium foil. The prepared cathode film was dried in a vacuum oven overnight, after which cathode discs were punched out and pressed. The active material loading is $1.5 \pm 0.2 \text{ mg cm}^{-2}$. Half cells were assembled in an argon-filled glovebox, with lithium foil as the anode and a

Powder Technology 363 (2020) 1–6.

porous polypropylene membrane (Celgard 2325) as the separator. The electrolyte used was LiPF_6 (1 M) in dimethyl carbonate (DEC) and ethylene carbonate (EC) (EC/DEC = 1:1 vol.%), purchased from Alfa Aesar. All assembled half-coin cells were left to settle for 10 hours before testing.

The electrochemical performance was tested using a charge-discharge study. Rate capacity tests were performed at different current rates ($1C = 180 \text{ mA/g}$), at room temperature over the potential range between 3.0 and 4.3 V using an Arbin battery tester. Cyclic voltammetry (CV) measurement was conducted in the range 2.8 to 4.3 V at a scanning rate of 0.1 mV/s. The electrochemical impedance spectroscopy (EIS) of the samples was performed in the frequency range from 0.005 Hz to 1 MHz. Both CV and EIS tests were done using a Gamry Reference 3000 Potentiostat/Galvanostat.

3. Results and discussion

Fig. 2 shows the XRD patterns of the synthesized powder samples. After heat treatment, both powders displayed a layered structure, identical to $\alpha\text{-NaFeO}_2$ -type [19]. The XRD spectra also show a separation between (018) and (110) peaks, implying that the synthesized powders have a well-ordered layered structure [20, 21]. The lattice parameters are shown in Table 1. The diffraction intensity ratios of $I_{(003)}/I_{(104)}$ for the FSP sample and the SD sample are 1.489 and 1.590, respectively. The intensity ratio provides qualitative information that the powders have a low order of cationic mixing [8, 9, 22].

Fig. 3 shows the SEM images of FSP and SD samples. It can be seen that both samples have wrinkled surface morphology. The morphology is associated with the droplet drying process shown in Fig. 4. At the early stage of the drying process, the solutes diffused slowly and got concentrated on the droplet surface, resulting in a supersaturated surface [23]. A soft but

impermeable shell was formed because of the increase in fluid viscosity [24, 25]. When the droplets were continuously heated and their temperature reached the boiling point, evaporation took place inside and inflated the droplets [26]. Once the pressure built up inside the droplets was sufficiently high, the outer shells might break and release the gas, leading to a porous and hollow structure [27]. Under the no-flame condition, the process was relatively slow and a rigid shell was formed during the inflation process and produced large porous particles with size mainly in the range of 20 – 40 μm . With flame, the particles were further processed and the soft shell collapsed before turning into a rigid shell, leaving relatively smaller particles of 10 – 20 μm . Different from the particles of the SD sample that are all porous, the FSP sample is a mixture of porous wrinkled particles and solid spherical particles. The mixed morphology is most likely caused by a non-uniform temperature field in the flame zone, where some powders were not fully heated due to a very short residence time (~ 1 ms). The morphology of the FSP powder could be further improved with a more uniform temperature field and a longer residence time for processing. From Fig. 3(e) and Fig. 3(f), we can also see that the primary particle size of the annealed powders is from 100 to 200 nm, the same in both cases, indicating that the post annealing process has a similar effect on crystal growth in these powders.

Fig. 5(a) shows the initial charge and discharge curves of coin cells using the two powders. The initial discharge capacity and the coulombic efficiency of the powder from the FSP process are 200.2 mAh/g and 83.4%, respectively. In contrast, the powder from the SD process has an initial discharge capacity and coulombic efficiency of 185.1 mAh/g and 82.7%, respectively. The increased capacity of the FSP powder is partially related to the change of the particle morphology. The values of the BET surface area of the FSD and SD powders are 3.536 $\text{m}^2 \text{g}^{-1}$ and 2.555 $\text{m}^2 \text{g}^{-1}$, respectively. Moreover, as observed in Fig. 3, the particle size of the FSD

powder is relatively smaller than that of the SD powder. The decreased particle size and increased BET surface area could result in a better diffusion of Li ions in the solid phase, leading to a higher discharge capacity of the FSD powder. Fig. 5(b) demonstrates the rate capability of FSP and SD powders. The rate changes from 0.1C to 5C with a cut-off voltage range of 3.0 – 4.3 V. At 0.1C, more significant capacity fade can be noticed in the SD sample. Whereas, when the C-rate increases further to 0.2C, 0.5C, 1C, 2C, 3C, and finally, 5C, no notable capacity fading is detected for both samples. The discharge capacity of the FSP sample at different rates was observed to be higher than that of the SD sample, except at 5C. At 5C, the FSP sample has an initial discharge capacity of 130.7 mAh/g, which is about the same as the SD sample at 130.9 mAh/g. This could be attributed to that the SD sample is more porous, resulting in a higher effective mass transfer between the electrode and the electrolyte that would be more pronounced at the highest rate [9]. After the high rate cycling and when the rate was returned to 0.1C, the FSP sample and the SD sample both have an excellent capacity retention rate of 98.4% and 96.2%, respectively.

The cyclic performance of powders at the rate of 1C is shown in Fig. 5(c). After 200 cycles, the capacity retention rate of the FSP sample and the SD sample is at 91.5% and 90.4%, respectively. These very high retention rates of the NCA powders, without any surface coatings, are attributed to the low cationic mixing in the powders during preparation [16]. As a matter of fact, the powders already formed a crystalline structure at low temperatures due to that the glycerol and the metal salts can form metal glycerolates [28]. It means that the cations were already locked into their positions, even at low temperatures during the spray synthesis. Furthermore, Fig. 5(d) shows cyclic performance at the rate of 5C. The capacity retention rates of the FSP sample and the SD sample are 89.4% and 85.4%, respectively, after 200 cycles.

The comparison between this work and other studies is listed in Table 2, which shows that our powders have a comparable initial capacity as other researcher's work. However, the rate capacities of our powders are extraordinary as compared to others, especially at high rates. The result shows that glycerol as the solvent for spraying processes could add additional benefits, such as ordering the crystalline structures at an early stage. Moreover, they show that the flame in the drying and pyrolysis processes is a key factor in contributing to capacity increase by reducing porosity.

The cyclic voltammetry (CV) results are shown in Fig. 6. For both powders from SD and FSP, the CV curves show three pairs of oxidation and reduction peaks, which are a typical feature of the NCA cathode material [29]. The first peak is for the phase transition from the pristine hexagonal phase to a monoclinic phase (H1 to M). The second peak is for the transition from the monoclinic phase to a second hexagonal phase (M to H2). The third peak corresponds to the transformation of the second hexagonal phase to a third hexagonal phase (H2 to H3) [4, 8, 30]. For the FSP sample, the CV curve of the first cycle shows cathodic/anodic peaks at 3.83 V/3.67 V for H1 to M, 4.00 V/3.97 V for M to H2, and 4.19 V/4.15 V for H2 to H3, respectively. There is no obvious change in the anodic peaks in the second and third cycles. Nevertheless, the cathodic peak of H1 to M changes notably from 3.83 V in the first cycle to 3.74 V in the second cycle, after which the peak changes slightly to 3.73 V in the third cycle. The change in the H1 to M peak is attributed to the phase transformation and formation of the solid electrolyte interphase (SEI) during the first cycle [9, 30]. Only very small changes in CV curves are observed in further cycles, indicative of a good reversible performance of the NCA powder.

In contrast, in the first charge-discharge cycle, the CV curve of the powder from SD process has cathodic/anodic peaks at 3.88 V/3.68 V for H1 to M, 4.00 V/3.95 V for M to H2, and 4.19

V/4.15 V for H2 to H3, respectively. In the second cycle, the cathodic peak of H1 to M shifts to 3.75 V, and further to 3.71 V in the third cycle. On the other hand, the anodic peaks are almost identical in all cycles for the two powders. The powder from the SD process was observed to experience more irreversible phase change, which implies that the SD powder has slower structural dynamics [31]. It is consistent with the charge-discharge results in Fig. 5 that shows the SD powder has a lower coulombic efficiency than the powder from the FSP process.

To further investigate the difference in the electrochemical performance of the two powders, electrochemical impedance spectroscopy (EIS) tests of the cells have been conducted. As shown in Fig. 7a, after 50 cycles, two semicircles are observed in the tested frequency range. The first semicircle represents the surface film resistance (R_f), which is the result of SEI formation, whereas the other one denotes charge transfer resistance (R_{ct}) [3, 32]. The values of R_f and R_{ct} after different cycles are listed in Table. 3. It can be seen that for both powders, R_f only increases slightly due to the growth of the SEI film. A higher surface film resistance is detected in the FSP powder than in the SD powder, implying that the SEI film may be thicker on the FSP powder [9, 33, 34]. In contrast, the charge transfer resistance of the SD powder is much larger than that of the FSP powders. The results indicate that the FSP powder has a better structural stability, which is attributed to its higher capacity retention ratio [8, 35].

4. Conclusions

The current study reported simple methods to synthesize NCA cathode material through flame assisted spray pyrolysis and spray drying using glycerol as the solvent. In general, the FSP process produced particles with smaller sizes, less wrinkled structure, and less porous morphology than that of the SD sample. The electrochemical tests show that the synthesized powder from FSP has an initial discharge capacity of 200.2 mAh/g at 0.1C, whereas the SD

Powder Technology 363 (2020) 1–6.

sample has an initial discharge capacity of 185.1 mAh/g at the same rate. Moreover, the FSP powder shows a better rate performance and higher capacity retention rates at both 1C and 5C. At 1C, it has a capacity retention rate of 91.5% after 200 cycles. Furthermore, it still has a capacity retention rate of 89.4% after 200 cycles at 5C, which is attributed to the early crystallization and structure ordering. The current work has demonstrated that using glycerol as a solvent is promising to synthesize NCA cathode material through spraying processes.

Acknowledgments

The authors would like to thank Dr. Eric Bohannon for obtaining XRD results. This material is based upon work supported by the Department of Energy, Office of Energy Efficiency and Renewable Energy (EERE), under Award Number DE-EE0007282.

References

- [1] A. Purwanto, C.S. Yudha, U. Ubaidillah, H. Widiyandari, T. Ogi, H. Haerudin, NCA cathode material: synthesis methods and performance enhancement efforts, *Materials Research Express*, 5 (2018) 122001.
- [2] J. Li, N. Zhang, H. Li, A. Liu, Y. Wang, S. Yin, H. Wu, J.R. Dahn, Impact of the Synthesis Conditions on the Performance of $\text{LiNi}_x\text{Co}_y\text{Al}_z\text{O}_2$ with High Ni and Low Co Content, *Journal of The Electrochemical Society*, 165 (2018) A3544-A3557.
- [3] S. Xia, F. Li, F. Cheng, X. Li, C. Sun, J.-J. Liu, G. Hong, Synthesis of Spherical Fluorine Modified Gradient Li-Ion Battery Cathode Material $\text{LiNi}_{0.80}\text{Co}_{0.15}\text{Al}_{0.05}\text{O}_2$ by Simple Solid Phase Method, *Journal of The Electrochemical Society*, 165 (2018) A1019-A1026.

Powder Technology 363 (2020) 1–6.

- [4] Z. Qiu, Y. Zhang, P. Dong, S. Xia, Y. Yao, A facile method for synthesis of $\text{LiNi}_{0.8}\text{Co}_{0.15}\text{Al}_{0.05}\text{O}_2$ cathode material, *Solid State Ionics*, 307 (2017) 73-78.
- [5] Q. Jiang, Y. Gao, J. Peng, H. Li, Q. Liu, L. Jiang, X. Lu, A. Hu, Effects of polyvinyl alcohol on the electrochemical performance of $\text{LiNi}_{0.8}\text{Co}_{0.15}\text{Al}_{0.05}\text{O}_2$ cathode material, *Journal of Solid State Electrochemistry*, 22 (2018) 3807-3813.
- [6] P. Dong, S. Xia, Y. Zhang, Y. Zhang, Z. Qiu, Y. Yao, Influence of complexing agent on the structure and electrochemical properties of $\text{LiNi}_{0.8}\text{Co}_{0.15}\text{Al}_{0.05}\text{O}_2$ cathode synthesized by sol-gel method: a comparative study, *Int. J. Electrochem. Sci.*, 12 (2017) 561-575.
- [7] T. Subburaj, Y.N. Jo, K. Prasanna, K.J. Kim, C.W. Lee, Titanium oxide nanofibers decorated nickel-rich cathodes as high performance electrodes in lithium ion batteries, *Journal of Industrial and Engineering Chemistry*, 51 (2017) 223-228.
- [8] P. Xiao, T. Lv, X. Chen, C. Chang, $\text{LiNi}_{0.8}\text{Co}_{0.15}\text{Al}_{0.05}\text{O}_2$: Enhanced Electrochemical Performance From Reduced Cationic Disorder in Li Slab, *Scientific Reports*, 7 (2017) 1408.
- [9] Y. Chen, P. Li, S. Zhao, Y. Zhuang, S. Zhao, Q. Zhou, J. Zheng, Influence of integrated microstructure on the performance of $\text{LiNi}_{0.8}\text{Co}_{0.15}\text{Al}_{0.05}\text{O}_2$ as a cathodic material for lithium ion batteries, *RSC Advances*, 7 (2017) 29233-29239.
- [10] G.D. Park, Y. Chan Kang, Characteristics of precursor powders of a nickel-rich cathode material prepared by a spray drying process using water-soluble metal salts, *RSC Advances*, 4 (2014) 44203-44207.
- [11] S.H. Ju, J.H. Kim, Y.C. Kang, Electrochemical properties of $\text{LiNi}_{0.8}\text{Co}_{0.2-x}\text{Al}_x\text{O}_2$ ($0 \leq x \leq 0.1$) cathode particles prepared by spray pyrolysis from the spray solutions with and without organic additives, *Metals and Materials International*, 16 (2010) 299-303.

Powder Technology 363 (2020) 1–6.

[12] J.H. Kim, Y.C. Kang, Electrochemical Properties of Nanosized $\text{Li}_2\text{MnO}_3 \cdot \text{Li}(\text{Ni}_{0.8}\text{Co}_{0.15}\text{Al}_{0.05})\text{O}_2$ Composite Cathode Powders, *Int J Electrochem Sci*, 8 (2013) 3664-3675.

[13] Y.S. Jang, J.H. Kim, J.-K. Lee, B.K. Park, Y.C. Kang, Electrochemical Properties of $0.6 \text{Li}_2\text{MnO}_3 \cdot 0.4 \text{Li}(\text{Ni}_{0.8}\text{Co}_{0.15}\text{Al}_{0.05})\text{O}_2$ Composite Nanopowders Prepared by Spray Pyrolysis, *Int. J. Electrochem. Sci*, 7 (2012) 12370-12382.

[14] S.H. Ju, H.C. Jang, Y.C. Kang, Al-doped Ni-rich cathode powders prepared from the precursor powders with fine size and spherical shape, *Electrochimica Acta*, 52 (2007) 7286-7292.

[15] H. Yang, P. Liu, Q. Chen, X. Liu, Y. Lu, S. Xie, L. Ni, X. Wu, M. Peng, Y. Chen, Y. Tang, Y. Chen, Fabrication and characteristics of high-capacity $\text{LiNi}_{0.8}\text{Co}_{0.15}\text{Al}_{0.05}\text{O}_2$ with monodisperse yolk-shell spherical precursors by a facile method, *RSC Advances*, 4 (2014) 35522-35527.

[16] K.I. Hamad, J.-Y. Liao, T.W. Smith, Y. Xing, Synthesis of Layered $\text{LiMn}_{1/3}\text{Ni}_{1/3}\text{Co}_{1/3}\text{O}_2$ Oxides for Lithium-Ion Batteries using Biomass-Derived Glycerol as Solvent, *Energy Technology*, 6 (2018) 710-717.

[17] K.I. Hamad, Y. Xing, Effect of Cobalt and Nickel Contents on the Performance of Lithium Rich Materials Synthesized in Glycerol Solvent, *Journal of The Electrochemical Society*, 165 (2018) A2470-A2475.

[18] N. Rahmat, A.Z. Abdullah, A.R. Mohamed, Recent progress on innovative and potential technologies for glycerol transformation into fuel additives: A critical review, *Renewable and Sustainable Energy Reviews*, 14 (2010) 987-1000.

Powder Technology 363 (2020) 1–6.

- [19] Z.-R. Chang, X. Yu, H.-W. Tang, X.-Z. Yuan, H. Wang, Synthesis of $\text{LiNi}_{1/3}\text{Co}_{1/3}\text{Al}_{1/3}\text{O}_2$ cathode material with eutectic molten salt LiOH-LiNO_3 , Powder Technology, 207 (2011) 396-400.
- [20] G. Hu, W. Liu, Z. Peng, K. Du, Y. Cao, Synthesis and electrochemical properties of $\text{LiNi}_{0.8}\text{Co}_{0.15}\text{Al}_{0.05}\text{O}_2$ prepared from the precursor $\text{Ni}_{0.8}\text{Co}_{0.15}\text{Al}_{0.05}\text{OOH}$, Journal of Power Sources, 198 (2012) 258-263.
- [21] P.S. Kumar, A. Sakunthala, M.V. Reddy, S. Shanmugam, M. Prabu, Correlation between the structural, electrical and electrochemical performance of layered $\text{Li}(\text{Ni}_{0.33}\text{Co}_{0.33}\text{Mn}_{0.33})\text{O}_2$ for lithium ion battery, Journal of Solid State Electrochemistry, 20 (2016) 1865-1876.
- [22] P. Yue, Z. Wang, W. Peng, L. Li, W. Chen, H. Guo, X. Li, Spray-drying synthesized $\text{LiNi}_{0.6}\text{Co}_{0.2}\text{Mn}_{0.2}\text{O}_2$ and its electrochemical performance as cathode materials for lithium ion batteries, Powder Technology, 214 (2011) 279-282.
- [23] I. Taniguchi, N. Fukuda, M. Konarova, Synthesis of spherical LiMn_2O_4 microparticles by a combination of spray pyrolysis and drying method, Powder Technology, 181 (2008) 228-236.
- [24] R. Vehring, Pharmaceutical Particle Engineering via Spray Drying, Pharmaceutical Research, 25 (2008) 999-1022.
- [25] C. Anandharamakrishnan, Spray drying techniques for food ingredient encapsulation, John Wiley & Sons, 2015.
- [26] C. Wan, M. Wu, D. Wu, Synthesis of spherical LiMn_2O_4 cathode material by dynamic sintering of spray-dried precursors, Powder Technology, 199 (2010) 154-158.
- [27] A. Gurav, T. Kodas, T. Pluym, Y. Xiong, Aerosol Processing of Materials, Aerosol Science and Technology, 19 (1993) 411-452.

Powder Technology 363 (2020) 1–6.

[28] P.-C. Lau, T.-L. Kwong, K.-F. Yung, Effective heterogeneous transition metal glycerolates catalysts for one-step biodiesel production from low grade non-refined *Jatropha* oil and crude aqueous bioethanol, *Scientific Reports*, 6 (2016) 23822-23822.

[29] C. Cao, J. Zhang, X. Xie, B. Xia, A novel method for the modification of $\text{LiNi}_{0.8}\text{Co}_{0.15}\text{Al}_{0.05}\text{O}_2$ with high cycle stability and low pH, *Journal of Solid State Electrochemistry*, 23 (2019) 1351-1358.

[30] H. Xie, K. Du, G. Hu, J. Duan, Z. Peng, Z. Zhang, Y. Cao, Synthesis of $\text{LiNi}_{0.8}\text{Co}_{0.15}\text{Al}_{0.05}\text{O}_2$ with 5-sulfosalicylic acid as a chelating agent and its electrochemical properties, *Journal of Materials Chemistry A*, 3 (2015) 20236-20243.

[31] L. Zhang, J. Fu, C. Zhang, Mechanical Composite of $\text{LiNi}_{0.8}\text{Co}_{0.15}\text{Al}_{0.05}\text{O}_2$ /Carbon Nanotubes with Enhanced Electrochemical Performance for Lithium-Ion Batteries, *Nanoscale Research Letters*, 12 (2017) 376.

[32] S.S. Zhang, K. Xu, T.R. Jow, Electrochemical impedance study on the low temperature of Li-ion batteries, *Electrochimica Acta*, 49 (2004) 1057-1061.

[33] C. Chen, M. Xu, K. Zhang, H. An, G. Zhang, B. Hong, J. Li, Y. Lai, Atomically ordered and epitaxially grown surface structure in core-shell NCA/ NiAl_2O_4 enabling high voltage cyclic stability for cathode application, *Electrochimica Acta*, 300 (2019) 437-444.

[34] M.M. Loghavi, H. Mohammadi-Manesh, R. Egra, $\text{LiNi}_{0.8}\text{Co}_{0.15}\text{Al}_{0.05}\text{O}_2$ coated by chromium oxide as a cathode material for lithium-ion batteries, *Journal of Solid State Electrochemistry*, 23 (2019) 2569-2578.

[35] H. Zhou, Z. Yang, D. Xiao, K. Xiao, J. Li, An electrolyte to improve the deep charge–discharge performance of $\text{LiNi}_{0.8}\text{Co}_{0.15}\text{Al}_{0.05}\text{O}_2$ cathode, *Journal of Materials Science: Materials in Electronics*, 29 (2018) 6648-6659.

Tables

Table 1. Lattice parameters of prepared NCA powders

Sample	a (Å)	c (Å)	c/a	R ($I_{(003)}/I_{(104)}$)
SD	2.8633	14.1835	4.9536	1.590
FSP	2.8630	14.1863	4.9550	1.489

Table 2. Comparison of results from this work and other spray methods

Synthesis method	Initial discharge capacity (mAh/g)	Potential range (V)	Capacity retention	Ref.
Ball Milling-Spray Drying	201.2 (0.1C)	2.8 – 4.3	79.08% after 100 cycles (5C)	[8]
Ball Milling-Spray Drying	205.1 (0.1C)	2.8 – 4.3	93.3% after 100 cycles (2C)	[9]
Two-step Spray Pyrolysis	200 (0.1C)	2.8 – 4.5	79.4% after 40 cycles (0.1C)	[14]
Two-step Spray Pyrolysis	218 (0.1C)	2.8 – 4.5	~100% after 20 cycles (0.1C)	[11]
SD using water	188 (at 100 mA/g)	2.8 – 4.5	94.7% after 100 cycles (100 mA/g)	[10]
FSP	168 (at 20 mA/g)	2.8 – 4.5	58% after 50 cycles (20 mA/g)	[12]
FSP	200.2 (0.1C)	3.0 – 4.3	94.2% after 100 cycle (1C) 94.1% after 100 cycle (5C)	This work

Table 3. Values of R_f and R_{ct} after different cycles.

Sample	Cycle number	R_f (Ω)	R_{ct} (Ω)
FSP	50	60.18	213.5
	100	67.81	256.3
	200	69.39	938.2
SD	50	52.88	337.1
	100	57.70	431.2
	200	61.31	1579.0

Figure captions

Fig. 1. Schematic of the spray based production process.

Fig. 2. XRD patterns of SD and FSP powders.

Fig. 3. SEM images at different magnifications of FSP (a, c, e) and SD (b, d, f) samples.

Fig. 4. Schematic of the particle formation process in spray drying and flame-assisted pyrolysis and drying.

Fig. 5. (a) Initial charge and discharge curves at 0.1C of the powders; (b) rate performance; (c) cyclic performance at 1C; (d) cyclic performance at 5C.

Fig. 6. CV results of (a) FSP and (b) SD powders.

Fig. 7. Nyquist plots of the NCA powders. (a) after 50 cycles, (b) after 100 cycles, and (c) after 200 cycles at 5C.

Fig. 1

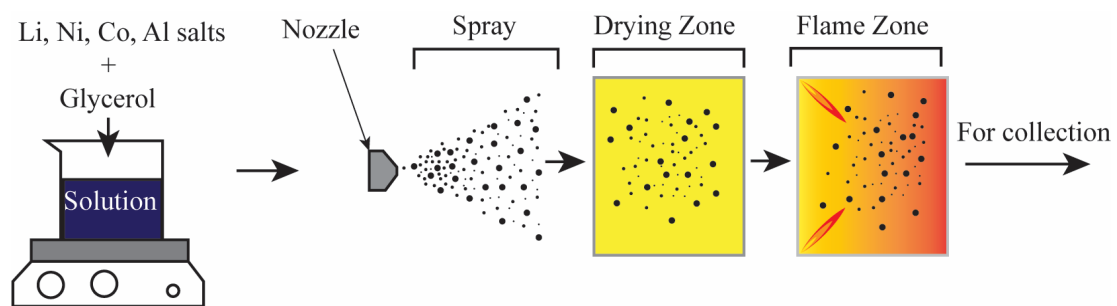


Fig. 2

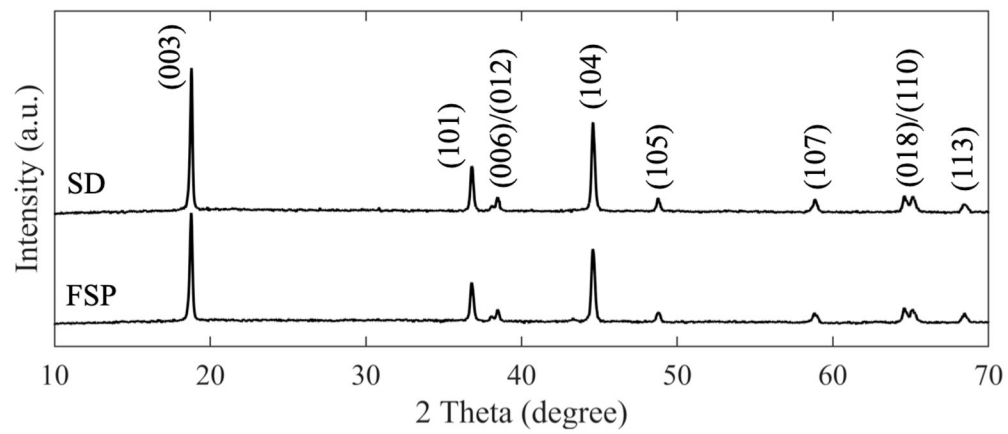


Fig. 3

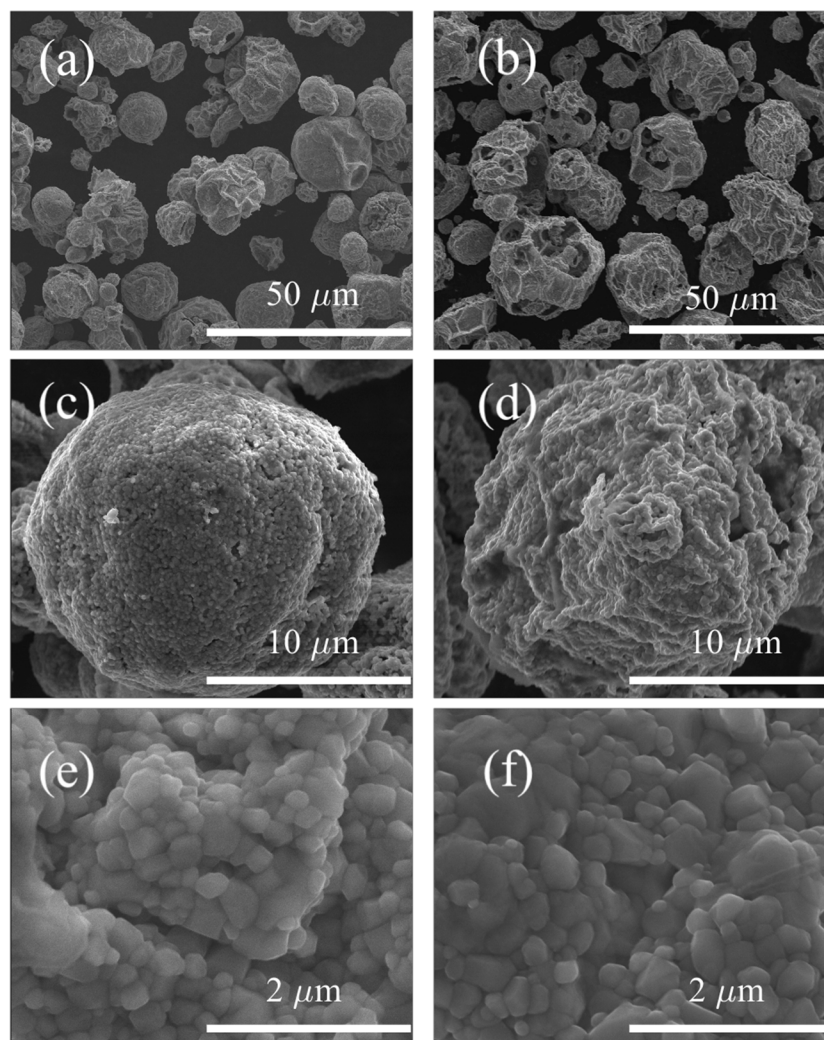


Fig. 4

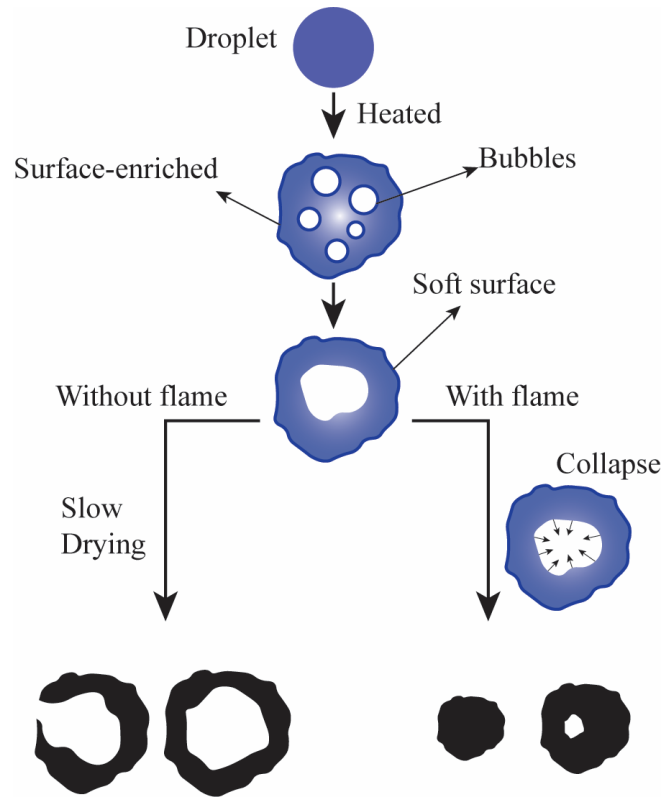


Fig. 5

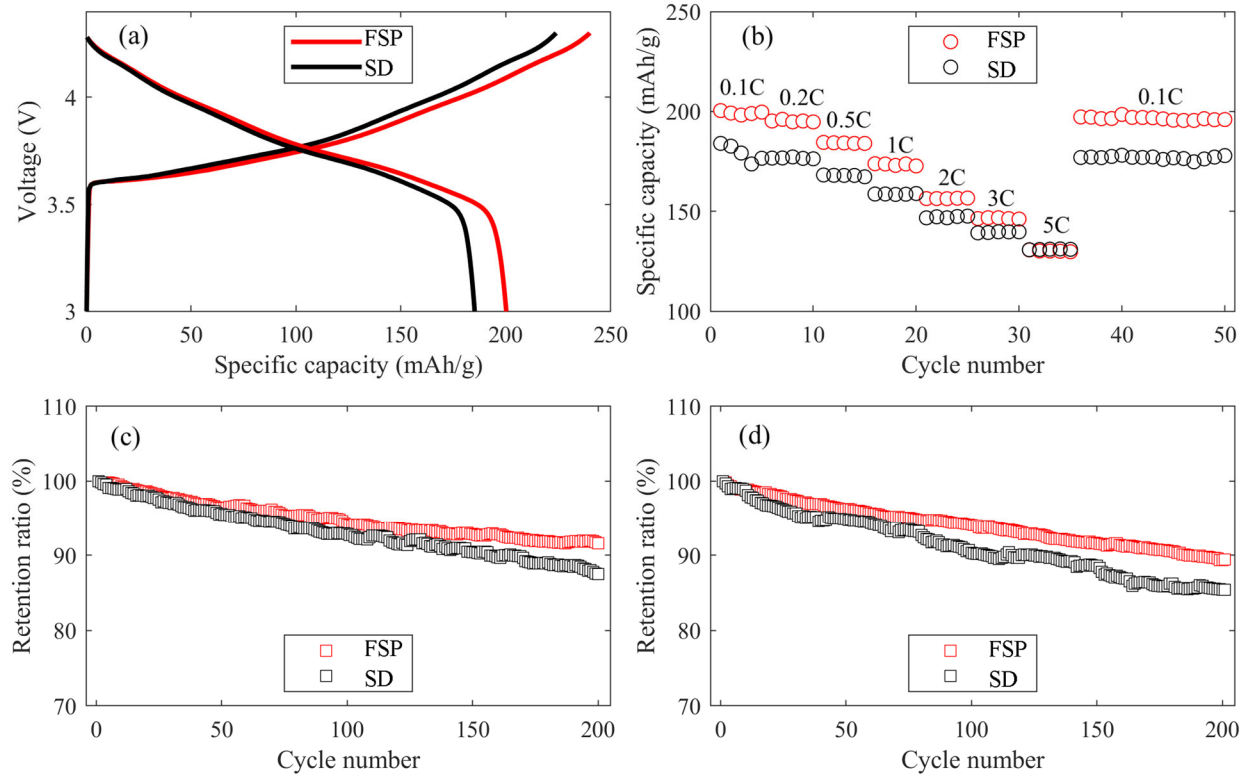


Fig. 6

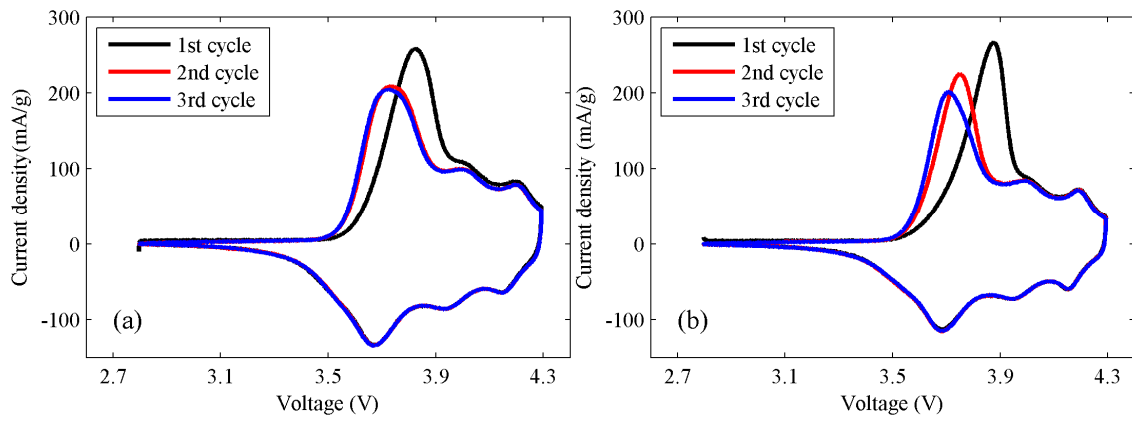


Fig. 7

